JMEPEG (2012) 21:936–945
DOI: 10.1007/s11665-011-9994-0

1059-9495/$19.00

Effect of Welding Parameters and Aging Process on the Mechanical Properties of Friction Stir-Welded 6063-T4 Al Alloy

Alaaddin Toktaş and Gülcan Toktaş

(Submitted March 1, 2010; in revised form May 5, 2011)

6063-T4 Al alloy was friction stir welded at various tool rotations (800, 1120, and 1600 rpm) and welding speeds (200 and 315 mm/min) using a specially manufactured tool with a height-adjustable and right-hand-threaded pin. The postweld aging process (at 185 °C for 7 h) was applied to a group of the welded plates. In this study, the effects of the welding parameters and the postweld aging treatment on the microstructural and mechanical properties of 6063-T4 Al alloy were studied. The maximum weld temperatures during the welding process were recorded, and the fracture surfaces of tensile specimens were examined using a scanning electron microscope. The homogeneous hardness profiles were obtained for all the weldings with no trace of softening regions. It was observed that the ultimate tensile strengths (UTS) increased slightly (on average by approx. 8%) and the percent elongations decreased (on average by approx. 33%) by the postweld aging treatment. The maximum bending forces (F_{max}) of all the welds were less than that of the base metal. It was observed that the F_{max} values increased after the postweld aging process at the welding speed of 315 mm/min and decreased at the welding speed of 200 mm/min.

Keywords friction stir welding, mechanical properties, postweld aging, 6063 Al alloy

1. Introduction

Friction stir welding (FSW) is a solid-state metal-joining method, which offers several advantages over conventional welding methods, including better mechanical properties, low residual stress, and reduced occurrence of defects (Ref 1). The process reduces manufacturing costs as a result of the elimination of some defects, filler materials, shielding gases, and costly weld preparation (Ref 2).

The basic principle of FSW is illustrated in Fig. 1. A non-consumable rotating tool with a specially designed pin and shoulder is inserted into the abutting edges of sheets or plates to be joined and traversed along the line of the joint. The tool serves the following two primary functions: first, to heat the workpiece, and second, to move the material to produce the joint (Ref 3-6). During this process, the frictional heat, which is generated by contact friction between the tool and the workpiece, softens the material. The plasticized material is stirred by the tool and forced to flow to the side and the back of the tool as the tool advances. As the temperature cools down, a solid continuous joint between the two plates is then formed (Ref 7, 8).

Precipitation hardening aluminum alloys are difficult to join by fusion welding techniques. They often lead to significant strength deterioration in the joints due to the dentritic structure formed in the fusion zone (Ref 9). The dissolution of the precipitate, which leads to unpinning and creates softening as well as grain coarsening, is another reason for the loss of mechanical properties. These alloys can be successfully joined by FSW technique in which no fusion zone is formed. There are some previous studies concerning the FSW of precipitation hardening aluminum alloys. Nelson and coworkers (Ref 10) studied the microstructural evolution (the grain structure, dislocation density and precipitation phenomena) at various regions of friction stir welded Al alloy 7050-T651 in detail. They reported that the dynamically recrystallized zone (DXZ) consisted of recrystallized, fine equiaxed grains, 1-4 μm in diameter, and contained a high dislocation density with varying degrees of recovery from grain to grain. Sato et al. (Ref 11) emphasized that the precipitates within the weld region (0-8.5 mm from the weld center) were completely dissolved into a 6063 aluminum matrix. They also reported that the hardness profile was strongly affected by precipitate distribution rather than grain size in the weld. Similarly, a complete dissolution of the precipitates in FSW of 6013 Al-T6 and T4 at a tool rotation speed of 1400 rpm and welding speeds of 400-450 mm/min was also reported by Heinz and Skrotzki (Ref 12).

Sato and Kokawa (Ref 2) conducted two different postweld treatments on the FSW samples of 6063 Al-T5 alloy with the thickness of 4 mm. The first was only an aging process at 175 °C for 12 h, while the second was both a solutionizing (at 530 °C for 1 h) and an aging (at 175 °C for 1 h) process. They concluded that the elongation, the yield, and the ultimate tensile strengths (UTS) were the lowest for the FSW samples, and the highest for both the solutionized and the aged conditions of FSW samples. In the case of the postweld aging process, the tensile properties were a bit more than that of the base metal.

In addition, previous studies have not considered the combined effects of the tool rotation speed, the welding speed,

Alaaddin Toktaş and **Gülcan Toktaş**, Department of Mechanical Engineering, Balıkesir University, 10145 Balıkesir, Turkey. Contact e-mail: atoktas@balikesir.edu.tr.

and the postweld treatment on the hardness, tensile and bending strengths of friction stir-welded workpieces. The aim of this study is to investigate the effect of the welding parameters (rotation speed and welding speed) and the postweld aging process on the microstructural and the mechanical properties (hardness, tensile, and bending) of the friction stir-welded Al alloy 6063-T4. In these experiments, measurement of the tensile fracture distances and examination of the fractured surfaces are also carried out.

2. Experimental Procedure

2.1 Work Material and Tool Preparation

The material used in this study is an extruded aluminum alloy 6063. The chemical composition is given in Table 1. The material was extruded to a plate of 3.70-mm thickness and 75-mm width. During the extrusion process, the material was solutionized at about 520 °C. After waiting at room temperature for a while, the plates were friction stir welded at various rotation and welding speeds. Some mechanical properties of the Al alloy 6063-T4 (base metal) are listed in Table 2.

A special stirring tool was designed and manufactured as part of the research (Ref 13). The tool, machined from DIN 1.2714 steel, was austenitized at 880 °C, quenched in oil, and tempered at 300 °C, having a hardness value of 45 HRc. An M6 × 0.75-mm right-hand-threaded pin, characterized by a hardness of 62 HRc, was used for joining the plates. The technical drawings of the shoulder and the pin, together with the solid pattern of the tool, are illustrated in Fig. 2. The

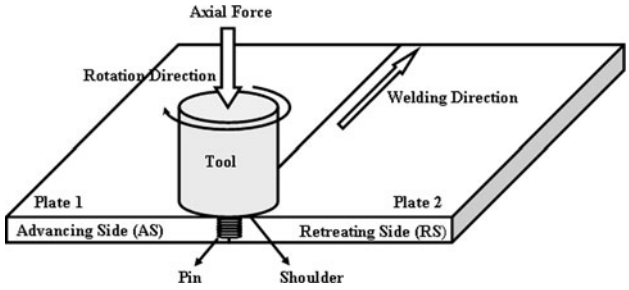

Fig. 1 Schematic drawing of FSW

Table 1 Chemical composition of aluminum alloy 6063-T4 (wt.%)

Si	Fe	Cu	Mn	Mg	Zn	Ti	Cr	Al
0.439	0.195	0.004	0.029	0.479	0.007	0.013	0.003	Bal

Table 2 Mechanical properties of Al alloy 6063-T4

Hardness, HV	Yield strength, MPa	Ultimate tensile strength, MPa	Percent elongation, %	Max. bending force, N
49	99.31	146.09	18.71	1324.35

proportion of the shoulder and the pin diameter was selected as 3:1. The plunge depth of the pin can be adjustable according to the thickness of the plate; this allows for multiple usages of the same tool for plates of different materials and various plate thicknesses (up to 10 mm) unless any deformation has been detected on the tool.

2.2 Welding

The plates (750 × 75 × 3.7 mm in dimensions) were butt friction stir welded using a clamping fixture to fix the plates onto the milling machine. During the welding process, some parameters were kept constant, such as tilt angle (2°) and tool rotation direction (clockwise). The welding direction was parallel to the extrusion direction, and the tool sinking into the plates was 3.55 mm. The rotation and the welding speeds used in this study are presented in Table 3. In order to obtain sound welds, they were selected according to the previous studies (Ref 14-16) and technical properties of the milling machine. Revolutionary pitches (RP = welding speed/rotation speed) and welding codes used for identifying the welds in this study are also shown in Table 3. During the welding process, the temperature variations were measured as nearly as possible to the weld center (approximately 10 mm behind the shoulder) by fixing a Raytek Pm Plus pyrometer to the spindle head of the milling machine. The maximum weld temperatures are given in Table 3 for all the welded plates. The temperature-time graphs were recorded using a Datatemp program, an example of which is given in Fig. 3 for B1 weld. Two welds were performed for each welding condition, and one of them was postweld aged at 185 °C for 7 h.

2.3 Mechanical Testing

In order to obtain the smooth surfaces and to prepare potential standard specimens, the upper surfaces of the 3.70-mm thick welded plates were machined to 3-mm thickness on a milling machine (using a cooling medium). 30 mm from both the beginning and the end of the plates was removed. Five tensile and bending specimens were cut out of each welded plate. Owing to the relatively large temperature variations throughout the weld (Fig. 3), the same kinds of specimens were cut from the same parts of the welded plates to minimize the effect of temperature variation on mechanical properties.

Tensile specimens were prepared according to the TS 287 EN 895 (Ref 17) with the tensile direction being perpendicular to the welding direction, so that the weld zone could be located in the middle of the specimen. Figure 4 shows the geometry of the tensile specimen. The tensile tests were performed at a nominal strain rate of 3.3×10^{-4} s^{-1} on the Shimadzu testing machine. The yield strengths, the UTS, and the percent elongation values were recorded. The fracture locations and distances from the weld center were also obtained for the as-welded and postweld aged plates.

For three point bending tests, specimens with the dimensions 150 mm × 20 mm × 3 mm were prepared perpendicular to the welding direction. These specimens were subjected to 180° bending tests. The tests were performed at a bending speed of 1 mm/min. The bending ratio was fixed at 4:1. The maximum bending force was recorded during tests.

The Vickers microhardness measurements were taken from the centerline on the cross section of the welds by using an Otto Wolpert-Werke hardness tester at 1 kgf load for 15 s.

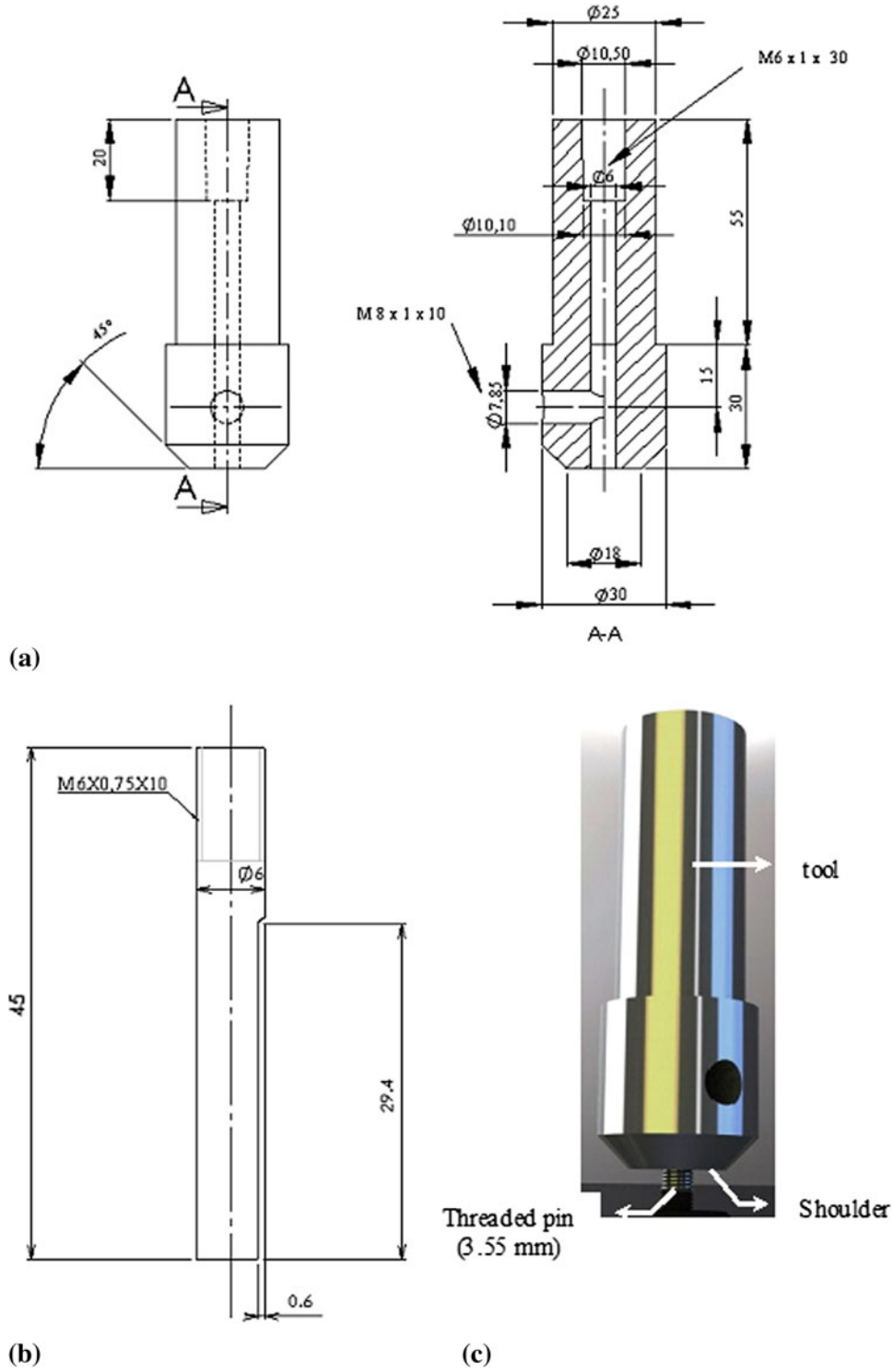

Fig. 2 Technical drawing of (a) the shoulder, (b) the pin, and (c) solid pattern of the tool

2.4 Microstructural Observation and Fractography

The as-welded and the postweld aged cross sections were polished with an alumina suspension, etched with Keller's reagent (150 mL H_2O, 3 mL HNO_3, 6 mL HF, and 6 mL HCl) and observed using an optical microscopy. The tensile-fractured surfaces were examined using a scanning electron microscope (SEM) for the 1600 rpm-200 mm/min and 800 rpm-315 mm/min welding conditions. It is reported (Ref 18) that increasing the rotation speeds or decreasing the travel (welding) speeds tends to increase the heat input and welding temperatures. Therefore, the 1600 rpm-200 mm/min welding case is considered as the highest heat input welding condition; 800 rpm-315 mm/min is considered as the lowest heat input welding condition in this study.

Table 3 Welding parameters, maximum weld temperatures, welding codes, fracture locations, and distances from the weld center

Rotation speed, rpm	Welding speed, mm/min	Revolutionary pitch, mm/rpm	Maximum weld temperature, °C	Welding codes	Fracture locations	Distances from the weld center, mm
800	200	0.25	473	A1	RS(a)	21
				PWA1	RS	19
	315	0.40	439	A2	AS(b)	15
				PWA2	RS	17
1120	200	0.18	478	B1	RS	22
				PWB1	RS	17
	315	0.28	472	B2	RS	20
				PWB2	RS	16
1600	200	0.125	513	C1	RS	26
				PWC1	RS	17
	315	0.20	489	C2	RS	20
				PWC2	RS	16

"PW" abbreviation indicates the postweld aged (185 °C for 7 h) condition
(a) Retreating side. (b) Advancing side

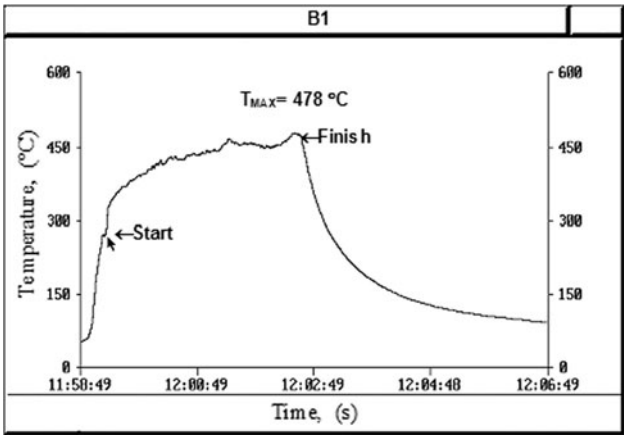

Fig. 3 Temperature-time graph for B1 weld

3. Results and Discussion

3.1 Macro and Microstructure

The macrostructures of A1 and PWA1 welds are shown in Fig. 5. These welds are considerably consistent with those found by other authors (Ref 2, 19, 20). Labels A, B, and C represent the weld nugget (WN) or the stir zone (SZ), the thermomechanically affected zone (TMAZ), and the heat-affected zone (HAZ), respectively. The unaffected zone of the weld is displayed as the base metal (BM). The WN widens near the upper surface in contact with the rotating head-pin fixture. This is because the upper surface experiences significantly high frictional heating and plastic flow due to contact with the shoulder of the tool during FSW. The size and the shape of the weld zone are almost the same for the as-welded and the postweld aged specimens, as seen in Fig. 5.

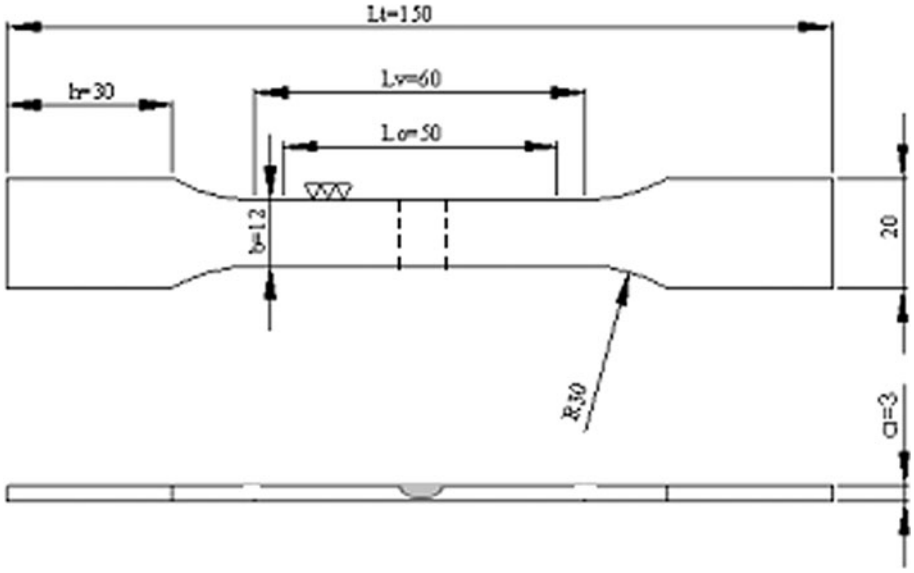

Fig. 4 Geometry of the tensile specimen

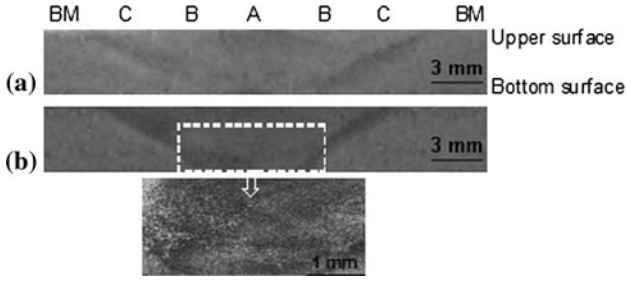

Fig. 5 Macrostructures of the cross sections perpendicular to the welding directions of (a) A1 and (b) PWA1 welds

Figure 6 shows the microstructures of the WNs for each welding. It can be seen that as the rotation speed increases at a constant welding speed, in general the grain sizes of the WNs increase clearly. A similar result was obtained by Xu et al. (Ref 21). If the microstructures are compared with respect to welding speed, no significant variation is seen in the grain sizes of the WNs. For this reason, it can be concluded that rotation speeds used in this study are more effective for the grain sizes of the WNs than the applied welding speeds. This can be attributed to the high welding temperatures obtained by the high rotation speeds. As presented in Table 3, high rotation speeds generally created high welding temperatures. This result is consistent with the previous study (Ref 22).

Some dark lines are observed in almost every microstructure of the WNs (Fig. 6). According to the literature (Ref 23), this appears to be a remnant of the joint-line that has sometimes been termed as the "Lady S" structure. Sato et al. (Ref 24) suggested that the initial oxide layer on the butt surface, fragmented during the FSW, was locally distributed as oxide particles on a zigzag line on the cross section. They reported that the zigzag line hardly influenced the mechanical properties.

3.2 Mechanical Properties

The horizontal hardness profiles of the as-welded and the postweld aged plates are shown in Fig. 7. Both groups of welds have roughly homogeneous hardness profiles as had been reported earlier by Sato et al. (Ref 22, 25) and Rodrigues et al. (Ref 26) for friction stir-welded Al alloys 5083-0, 6063-T4 and 6016-T4, respectively. In contrast, similar research studies (Ref 27-29) observed low hardness regions at the WN or at TMAZ. This contradiction can be attributed to many variables including welding process parameters, hardness measurement methods, production, and initial temper condition of the base metal. For instance, Sato et al. (Ref 22) studied on Al alloy 6063-T5 and T4, and they obtained a low hardness (softened) region for T5 and an homogeneous hardness profile for the T4 initial temper condition.

The reason for the non-softening region or the increase in the hardness of the WN can be explained by the weld temperature during welding. As can be seen in Table 3, the maximum weld temperatures almost reach the solutionizing temperature of 6063 alloy. Thus, during the welding process, the WN region is exposed to solutionizing treatment and in that region the existing second phase particles are dissolved, making the region free of precipitate. After a while, natural aging process may take place in this free precipitate region, causing an increase in hardness. This result is consistent with the previous study (Ref 30).

The hardness values obtained are in the range of 40-56 HV for the as-welded condition (Fig. 7a). It is found that the hardness values of the welds, performed at 200 mm/min welding speed, are slightly higher than the welds performed at 315 mm/min. In addition, the hardness values increased as the rotation speed increased for the as-welded condition.

By the postweld aging process, the hardness values obtained are mostly less than the hardness of the base metal, which has a value of 49 HV (Fig. 7b). In comparison with the as-welded condition, the welds performed at 315 mm/min welding speed exhibited higher hardness values than those when treated at 200 mm/min. In common with the as-welded condition, the hardness values are increased by the rotation speeds. This increase is more apparent for the 200 mm/min welding speed.

Comparing the hardness profiles of the as-welded and the postweld aged plates (Fig. 7a, b), slight reductions are observed in the hardness values for the postweld aged condition. Sato et al. (Ref 22) reported that postweld aging at 175 °C for 12 h had increased the hardness value of the welded Al alloy 6063-T4 from 45 to 85 HV. This contradiction can be attributed to the difference between the aging conditions, which, in this study, is 185 °C for 7 h.

The variation in the tensile properties due to the welding parameters (rotation and welding speed) for the as-welded and the postweld aged conditions is presented in Fig. 8. Depending on the welding speed and the postweld aged conditions, the effect of the rotation speed on the tensile properties was different. The yield and the UTS decreased slightly because of the rotation speed for the welds performed at 315 mm/min welding speed. In the case of 200 mm/min welding speed, the strengths increased slightly with the increase of the rotation speed. Xu et al. (Ref 21) found a similar result; that the tensile, yield strengths and elongation values had increased linearly with increasing rotation speed from 800 to 1100 rpm at a constant welding speed of 140 mm/min. In general, the yield strength and the UTS increased with increase in rotation speed for the postweld aged plates.

It was observed that the high rotation speed (1600 rpm) removed the effect of the welding speed for the as-welded condition. The yield, the UTS, and the percent elongation values were measured equally for both the 200 and 315 mm/min welding speeds at 1600 rpm, as 100 MPa, 140 MPa, and 19%, respectively. At the low rotation speed (800 rpm), the strengths and the percent elongation increased with increasing welding speed. Hence, it can be concluded that the welding speed is not the solely determinant parameter on the tensile property, and the effect of the rotation speed should not be neglected. Ericsson and Sandstrom (Ref 31) welded the plates of 6082-T6 and 6082-T4 alloys at high rotation speeds (2200 and 2500 rpm) using various welding speeds between 700 and 1400 mm/min. They reported that the welding speed had no considerable effect on the tensile properties.

The yield strength, the UTS, and the percent elongation values obtained were higher for the welds performed at a 315 mm/min welding speed for both the as-welded and the postweld aged conditions. However, the postweld aging process at 185 °C for 7 h generally increased both the UTS and the yield strength (on average, at a ratio of 8 and 12%, respectively), but it decreased the percent elongation values (on average by 33%) of the welds.

The tensile-fractured locations and the distances of these locations from the weld centers are given in Table 3. It is observed that all the welds are fractured at the retreating sides

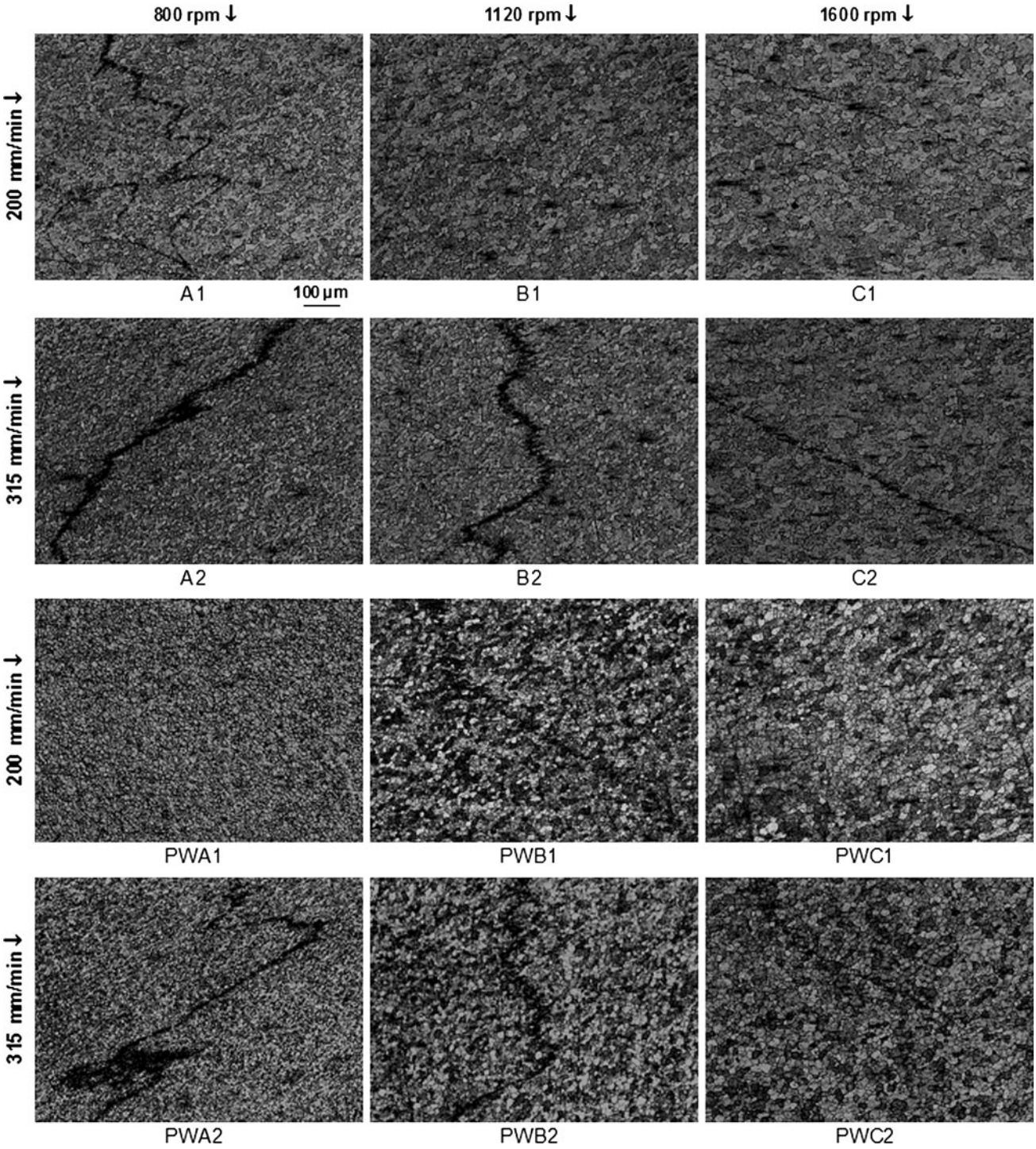

Fig. 6 Microstructures of the weld nuggets

except for the A2 weld. A similar observation was also made in previous studies (Ref 21, 32, 33). This result shows that the tensile properties of the advancing side may be better than the retreating side of the weld, and the properties of these two sides are not the same. Huijie et al. (Ref 34) reported that the tensile fractures were on the retreating side and the mechanical properties of the retreating side were poorer than that of the advancing side for 6061-T6 Al alloy. In contrast, some previous studies (Ref 14, 27, 29, 35) reported that tensile fractures occurred in the stir zone or on the advancing side because of localized defects or minimum hardness at the fracture locations.

The nearest fracture to the weld center was 15 mm for the A2 weld which was welded at 0.4 mm/rpm RP and had a 439 °C maximum weld temperature. The furthest fracture was obtained for the C1 weld, which had the highest weld temperature (513 °C) and the highest heat input. Furthermore, it appears that the fracture distances generally decrease or come close to the weld center by the applied postweld aging procedure.

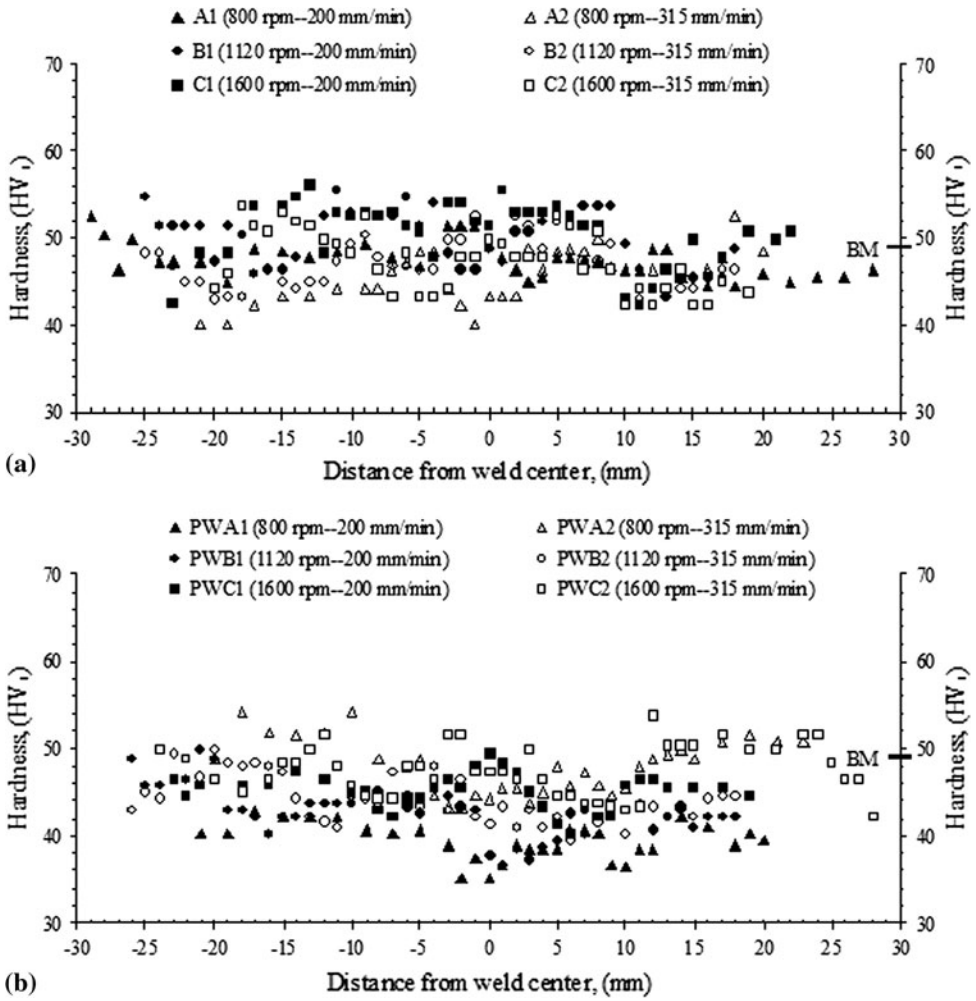

Fig. 7 Horizontal hardness profiles of the (a) welded and (b) postweld aged plates

No visible damage was observed in any of the welded specimens after 180° bending tests, as shown in Fig. 9. This endorses the result of the tensile tests in which the tensile fractures did not occur at the WNs. The variations of the UTS and the maximum bending forces (F_{max}) for the as-welded and the postweld aged specimens are presented in Fig. 10. In general, it is observed that the fluctuations of the maximum bending forces and the UTS are almost parallel to each other for both the as-welded and the postweld aged conditions. During bending, while the bottom surfaces of the specimens which correspond to the upper surface of the WN were subjected to tensile stress, the upper surfaces were subjected to compression stress. Therefore, parallel fluctuation between the bending forces and the UTS is an expected result.

It has also been found that the maximum bending forces of all the welds are less than that of the base metal (1324 N). The least bending force was measured for the weld, performed at 800 rpm-200 mm/min welding parameters and postweld aged condition, as 951 N, 373 N less than the bending force of the base metal. The highest F_{max} value (1275 N) was measured for PWB2 and PWC2 welds, only 49 N less than F_{max} of the base metal.

The F_{max} values increased slightly (9 N enhancement) at the welding speed at 1120 and 1600 rpm rotation speeds for the as-welded condition. On the other hand, the F_{max} values decreased after the postweld aging process for the welds, performed at 200 mm/min welding speed. The maximum reduction (147 N) was recorded between A1 and PWA1, welded at an 800 rpm tool rotation speed. In contrast, the postweld aging process caused the F_{max} values to increase at a welding speed of 315 mm/min. The maximum rising (167 N) is between A2 and PWA2, welded at 800 rpm. It can be concluded that the postweld aging process is more effective on the F_{max} value at the low rotation speed (800 rpm).

3.3 Fractography

The fractographies of the as-welded, the postweld aged, and BM tensile specimens are shown in Fig. 11. Only the graphs of specimens that were welded at the highest (1600 rpm-200 mm/min) and the lowest (800 rpm-315 mm/min) heat input welding conditions have been exhibited. The fracture mode is entirely ductile in manner with dimple formation for all the given welds and also for the base metal. Thomas and Nicholas (Ref 36) studied the fracture surface of friction stir-welded 50-mm-thick 6082-T6 aluminum alloy. They reported that the fracture type was ductile with microvoid coalescence mechanism both at the WN and base material.

No clear distinctions in fracture modes are seen between the fractographies of all the welded plates. In other words, neither

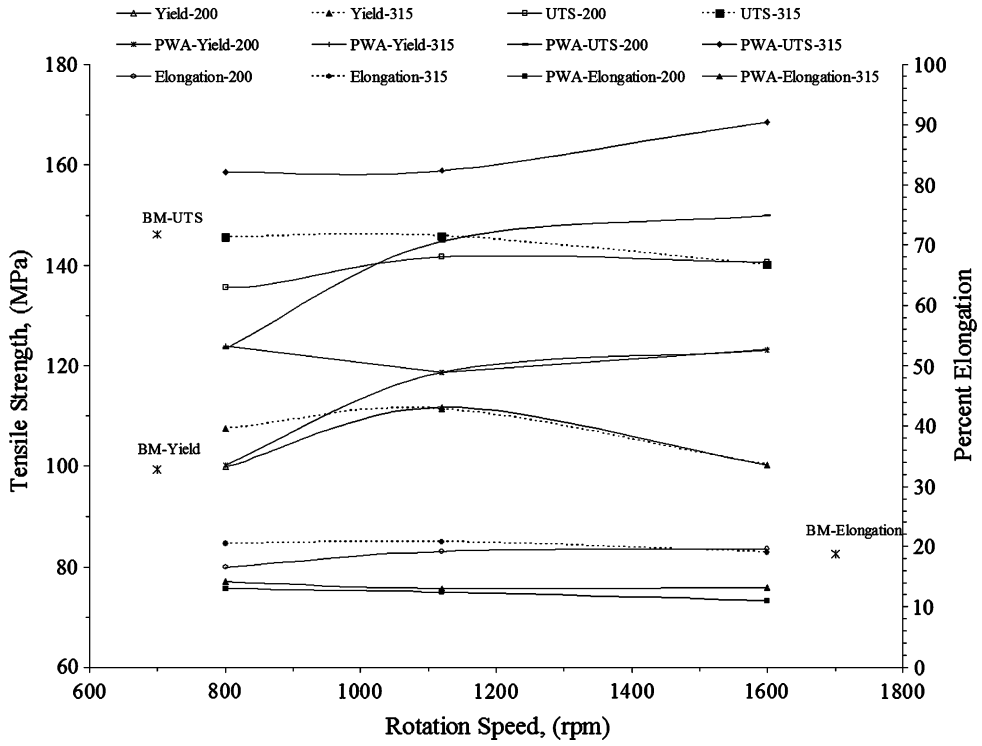

Fig. 8 Variation of the tensile properties of the welded and postweld aged plates due to the welding parameters

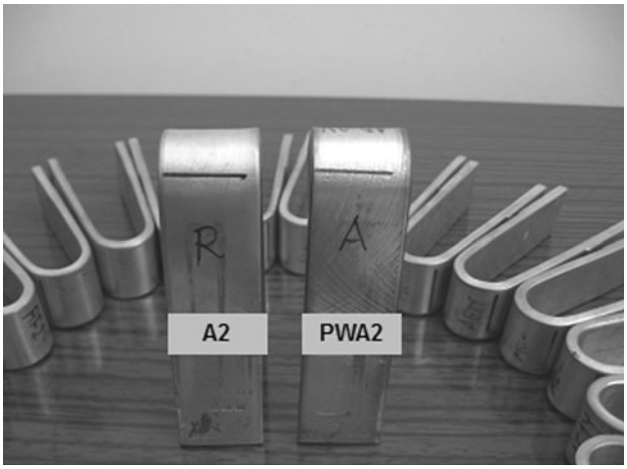

Fig. 9 Photograph of the bending specimens after 180° bending tests

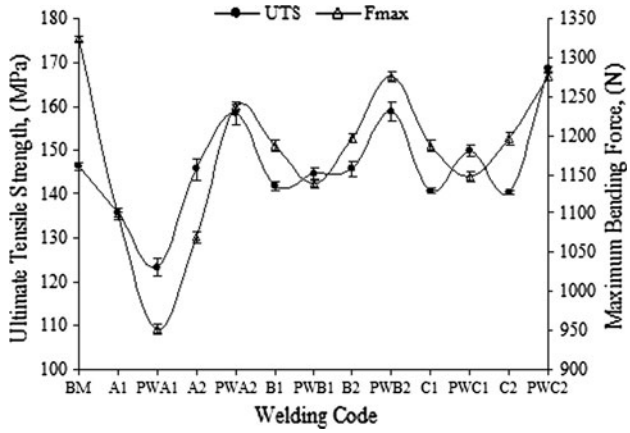

Fig. 10 Variations of the UTS and the maximum bending force

the low nor the high heat input welding conditions, which occurred at A2 and C1 welds, respectively, made any significant difference in the fracture mode. The postweld aging procedure did neither significantly influence the mechanical properties of 6063-T4 Al alloy nor distinctly affect the fracture modes.

4. Conclusions

In this study, the effects of the welding parameters and the postweld aging procedure on the microstructural and the mechanical properties of friction stir-welded aluminum alloy 6063-T4 were studied. Sound welds were carried out using a manufactured tool and selected welding parameters. Homogeneous hardness profiles were obtained for all the weldings with no softening regions. The hardness values increased with the rotation speed for both the as-welded and the postweld aged conditions. After the postweld aging process, the hardnesses decreased slightly, mostly below the hardness value of the base metal. The effect of the rotation speed on the tensile properties depended on the welding speed and the postweld aging process. The yield and the UTS were increased by the rotation speed at a low welding speed (200 mm/min) and/or the postweld aging process. The F_{max} values obtained were lower than the values of the base metal. In addition, the effect of the aging process on the bending force was dependent on the welding speed. The

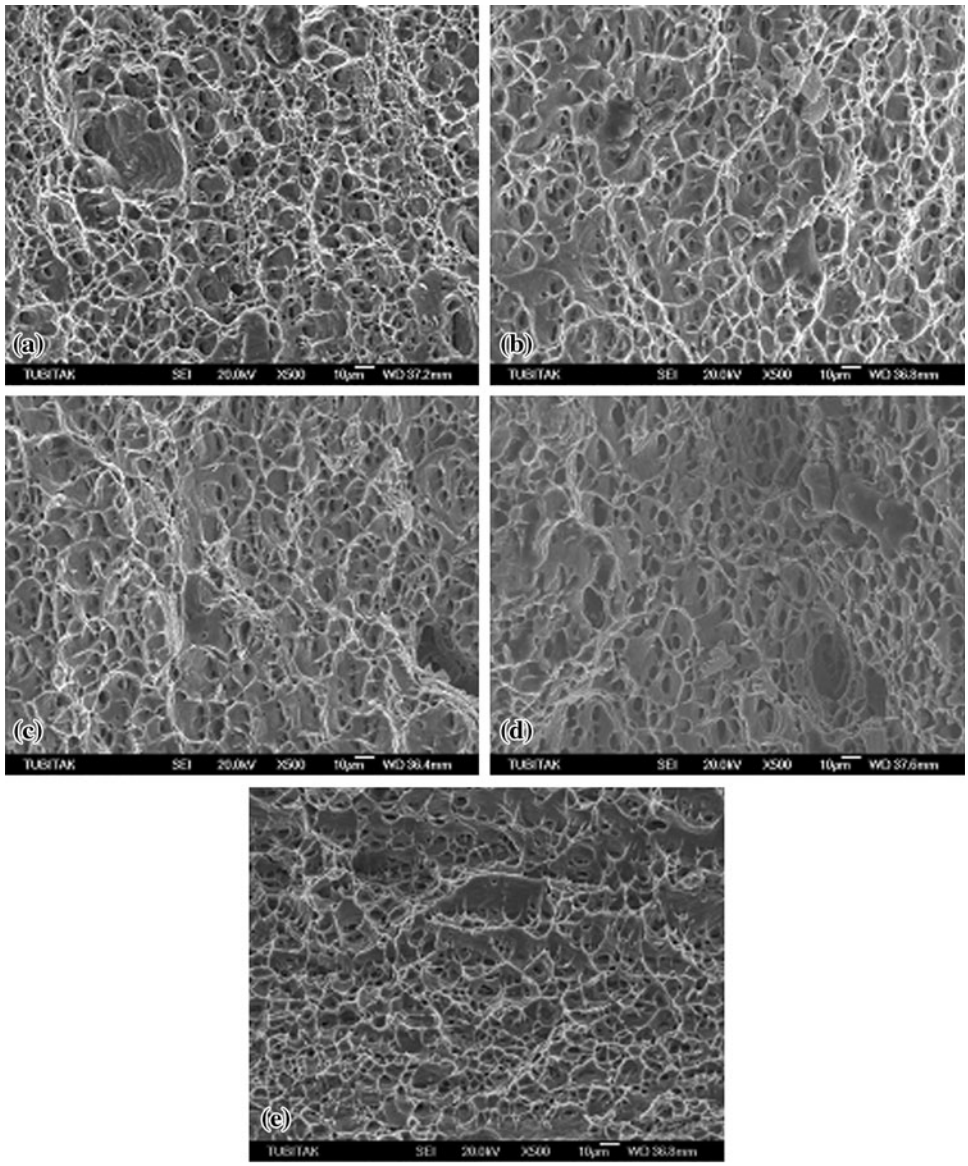

Fig. 11 Fracture surfaces of the specimens (a) A2, (b) C1, (c) PWA2, (d) PWC1, and (e) BM

F_{max} values decreased for the low welding speed (200 mm/min) and increased for the higher one (315 mm/min). In conclusion, all the tensile fractures occurred at the retreating sides of the welds and the postweld aging procedure caused the tensile fractures to come close to the weld center. The tensile fracture distances were 15-26 mm away from the weld centers. Consequently, a 315 mm/min welding speed was recommended over 200 mm/min, as it provided a higher yield, UTS, and bending forces. Furthermore, the postweld aging at 185 °C for 7 h made no satisfactory improvement on the observed mechanical properties.

Acknowledgments

The authors would like to express their most sincere gratitude and appreciation to the valuable help and cooperation extended by the Turkish Land Forces 6th Maintenance Central Commandership and Tekersan A.Ş. This research was supported by the Research Project Fund of Balikesir University.

References

1. S. Hong, S. Kim, C.G. Lee, and S.J. Kim, Fatigue Crack Behavior of Friction Stir Welded Al-Mg-Si Alloy, *Scripta Mater.*, 2006, **55**(11), p 1007–1010
2. Y.S. Sato and H. Kokawa, Distribution of Tensile Property and Microstructure in Friction Stir Weld of 6063 Aluminum, *Metall. Mater. Trans. A*, 2001, **32**(12), p 3023–3031
3. R.S. Mishra and Z.Y. Ma, Friction Stir Welding and Processing, *Mater. Sci. Eng. R*, 2005, **50**(1–2), p 1–78
4. C.G. Rhodes, M.W. Mahoney, and W.H. Bingel, Effects of Friction Stir Welding on Microstructure of 7075 Aluminum, *Scripta Mater.*, 1997, **36**(1), p 69–75
5. A. Barcellona, G. Bufa, L. Fratini, and D. Palmeri, On Microstructural Phenomena Occurring in Friction Stir Welding of Aluminium Alloys, *J. Mater. Proc. Technol.*, 2006, **177**(1–3), p 340–343

6. C. Meran, The Joint Properties of Brass Plates by Friction Stir Welding, *Mater. Des.*, 2006, **27**(9), p 719–726
7. X.K. Zhu and Y.J. Chao, Numerical Simulation of Transient Temperature and Residual Stresses in Friction Stir Welding of 304L Stainless Steel, *J. Mater. Proc. Technol.*, 2004, **146**(2), p 263–272
8. C.M. Chen and R. Kovacevic, Finite Element Modelling of Friction Stir Welding-Thermal and Thermomechanical Analysis, *Int. J. Mach. Tools Manuf.*, 2003, **43**(13), p 1319–1326
9. C. Genevois, A. Deschamps, A. Denquin, and B. Doisneau-cottignies, Quantitative Investigation of Precipitation and Mechanical Behaviour for AA 2024 Friction Stir Welds, *Acta Mater.*, 2005, **53**(8), p 2447–2458
10. J.-Q. Su, T.W. Nelson, R. Mishra, and M. Mahoney, Microstructural Investigation of Friction Stir Welded 7050-T651 Aluminium, *Acta Mater.*, 2003, **51**(3), p 713–729
11. Y.S. Sato, H. Kokawa, M. Enomoto, and S. Jogan, Microstructural Evolution of 6063 Aluminum During Friction-Stir Welding, *Metall. Mater. Trans. A*, 1999, **30**(9), p 2429–2437
12. B. Heinz and B. Skrotzki, Characterization of a Friction-Stir-Welded Aluminum Alloy 6013, *Metall. Mater. Trans. B*, 2002, **33**(3), p 489–498
13. A. Toktaş, "The Application of Friction Stir Welding on AA 6063 Aluminium Alloys and Investigating the Effect of the Welding Parameters on the Materials Microstructure and the Mechanical Properties," Ph.D. thesis, Balıkesir University, Institute of Science, 2006
14. K. Elangovan, V. Balasubramanian, and S. Babu, Predicting Tensile Strength of Friction Stir Welded AA6061 Aluminium Alloy Joints by a Mathematical Model, *Mater. Des.*, 2009, **30**(1), p 188–193
15. S. Rajakumar, C. Muralidharan, and V. Balasubramanian, Influence of Friction Stir Welding Process and Tool Parameters on Strength Properties of AA7075-T6 Aluminium Alloy Joints, *Mater. Des.*, 2011, **32**(2), p 535–549
16. M.S. Han, S.J. Lee, J.C. Park, S.C. Ko, Y.B. Woo, and S.J. Kim, Optimum Condition by Mechanical Characteristic Evaluation in Friction Stir Welding for 5083-0 Al Alloy, *Trans. Nonferrous Met. Soc. China*, 2009, **19**(s1), p 17–22
17. Destructive Tests on Welds in Metallic Materials-Transverse Tensile Test, TS 287 EN 895, April 1996
18. T. Khaled, An Outsider Looks at Friction Stir Welding, Report: ANM-112N-05-06, July 2005
19. W. Deqing, L. Shuhua, and C. Zhaoxia, Study of Friction Stir Welding of Aluminum, *J. Mater. Sci.*, 2004, **39**(5), p 1689–1693
20. G. Liu, L.E. Murr, C.S. Niou, J.C. McClure, and F.R. Vega, Microstructural Aspects of the Friction Stir Welding of 6061-T6 Aluminum, *Scripta Mater.*, 1997, **37**(3), p 355–361
21. W. Xu, J. Liu, G. Luan, and C. Dong, Microstructure and Mechanical Properties of Friction Stir Welded Joints in 2219-T6 Aluminum Alloy, *Mater. Des.*, 2009, **30**(9), p 3460–3467
22. Y.S. Sato, M. Urata, and H. Kokawa, Parameters Controlling Microstructure and Hardness During Friction-Stir Welding of Precipitation-Hardenable Aluminum Alloy 6063, *Metal. Mater. Trans. A*, 2002, **33**(3), p 625–635
23. T.L. Dickerson and J. Przydatek, Fatigue of Friction Stir Welds in Aluminium Alloys That Contain Root Flaws, *Int. J. Fatigue*, 2003, **25**(12), p 1399–1409
24. Y.S. Sato, F. Yamashita, Y. Sugiura, S.H.C. Park, and H. Kokawa, FIB-Assisted TEM Study of an Oxide Array in the Root of a Friction Stir Welded Aluminium Alloy, *Scripta Mater.*, 2004, **50**(3), p 365–369
25. Y.S. Sato, S.H.C. Park, and H. Kokawa, Microstructural Factors Governing Hardness in Friction Stir Welds of Solid-Solution-Hardened Al Alloys, *Metall. Mater. Trans. A*, 2001, **32**(12), p 3033–3042
26. D.M. Rodrigues, A. Loureiro, C. Leitao, R.M. Leal, B.M. Chaparro, and P. Vilaça, Influence of Friction Stir Welding Parameters on the Microstructural and Mechanical Properties of AA 6016-T4 Thin Welds, *Mater. Des.*, 2009, **30**(6), p 1913–1921
27. X.-G. Chen, M. da Silva, P. Gougeon, and L. St-Georges, Microstructure and Mechanical Properties of Friction Stir Welded AA6063-B4C Metal Matrix Composites, *Mater. Sci. Eng. A*, 2005, **518**(1–2), p 174–184
28. E. Cerri and P. Leo, Warm and Room Temperature Deformation of Friction Stir Welded Thin Aluminium Sheets, *Mater. Des.*, 2010, **31**(3), p 1392–1402
29. P.M.G.P. Moreira, F.M.F. de Oliveira, and P.M.S.T. de Castro, Fatigue Behaviour of Notched Specimens of Friction Stir Welded Aluminium Alloy 6063-T6, *J. Mater. Proc. Technol.*, 2008, **207**(1–3), p 283–292
30. S. Lim, S. Kim, C.G. Lee, and S. Kim, Tensile Behavior of Friction-Stir-Welded Al 6061-T651, *Metall. Mater. Trans. A*, 2004, **35**(9), p 2829–2835
31. M. Ericsson and R. Sandstrom, Influence of Welding Speed on the Fatigue of Friction Stir Welds and Comparison with MIG and TIG, *Int. J. Fatigue*, 2003, **25**(12), p 1379–1387
32. P.M.G.P. Moreira, T. Santos, S.M.O. Tavares, V. Richter-Trummer, P. Vilaça, and P.M.S.T. de Castro, Mechanical and Metallurgical Characterization of Friction Stir Welding Joints of AA6061-T6 with AA6082-T6, *Mater. Des.*, 2009, **30**(1), p 180–187
33. K. Elangovan and V. Balasubramanian, Influences of Tool Pin Profile and Welding Speed on the Formation of Friction Stir Processing Zone in AA2219 Aluminium Alloy, *J. Mater. Proc. Technol.*, 2008, **200**(1–3), p 163–175
34. L. Huijie, H. Fujii, M. Maeda, and K. Nogi, Tensile Properties and Fracture Locations of Friction-Stir Welded Joints of 6061-T6 Aluminum Alloy, *J. Mater. Sci. Lett.*, 2003, **22**(15), p 1061–1063
35. H. Aydın, A. Bayram, A. Uğuz, and K.S. Akay, Tensile Properties of Friction Stir Welded Joints of 2024 Aluminum Alloys in Different Heat-Treated-State, *Mater. Des.*, 2009, **30**(6), p 2211–2221
36. W.M. Thomas and E.D. Nicholas, Friction Stir Welding for the Transportation Industries, *Mater. Des.*, 1997, **18**(4), p 269–273